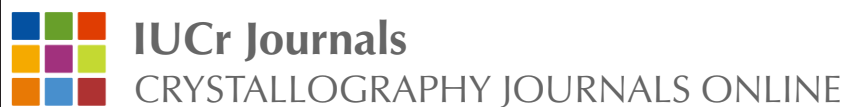


## Averaging the intensity of many-layered structures for accurate stacking-fault analysis using Rietveld refinement

Alan A. Coelho, John S. O. Evans and James W. Lewis

*J. Appl. Cryst.* (2016). **49**, 1740–1749



Copyright © International Union of Crystallography

Author(s) of this paper may load this reprint on their own web site or institutional repository provided that this cover page is retained. Republication of this article or its storage in electronic databases other than as specified above is not permitted without prior permission in writing from the IUCr.

For further information see <http://journals.iucr.org/services/authorrights.html>

# Averaging the intensity of many-layered structures for accurate stacking-fault analysis using Rietveld refinement

 Alan A. Coelho,<sup>a\*</sup> John S. O. Evans<sup>b</sup> and James W. Lewis<sup>b</sup>
<sup>a</sup>72 Cedar Street, Wynnum, Brisbane, Queensland 4178, Australia, and <sup>b</sup>Department of Chemistry, University Science Site, Durham University, South Road, Durham DH1 3LE, England. \*Correspondence e-mail: [alancoelho@bigpond.com](mailto:alancoelho@bigpond.com)

Received 2 June 2016

Accepted 12 August 2016

Edited by Th. Proffen, Oak Ridge National Laboratory, USA

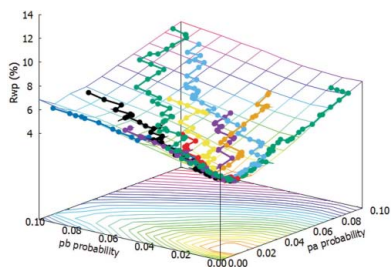
**Keywords:** stacking faults; Rietveld refinement; crystallography; *TOPAS* software.

Many technologically important synthetic and natural materials display stacking faults which lead to complex peak broadenings, asymmetries and shifts in their powder diffraction patterns. The patterns can be described using an enlarged unit cell (called a supercell) containing an explicit description of the layers. Since the supercell can contain hundreds of thousands of atoms with hundreds of thousands of *hkl* reflections, a Rietveld approach has been too computationally demanding for all but the simplest systems. This article describes the implementation of the speed-ups necessary to allow Rietveld refinement in the computer program *TOPAS* Version 6 (Bruker AXS, Karlsruhe, Germany). Techniques implemented include: a peaks buffer that allows hundreds of thousands of *hkl*-dependent peak shapes to be automatically approximated by a few hundred peaks; an averaging process for hundreds of large supercells with minimum impact on computational time; a smoothing technique that allows for the use of small supercells which approximate supercells ten to 20 times larger; and efficient algorithms for stacking sequence generation. The result is Rietveld refinement of supercells operating at speeds several thousand times faster than traditional Rietveld refinements. This allows quantitative and simultaneous analysis of structure and microstructure in complex stacking-faulted samples.

## 1. Introduction

Quantitative Rietveld analysis of layered structures exhibiting stacking vector faulting is becoming more common as computers become more powerful and the analytical software more accommodating. The supercell approach (Ufer *et al.*, 2004; Wang *et al.*, 2012; Lutterotti *et al.*, 2010) uses multiple layers in an enlarged unit cell in order to simulate faulted layered structures; it was used alongside recursive *DIFFaX* simulations (Treacy *et al.*, 1991) using *TOPAS* Version 5 by Bette *et al.* (2015). In that work many stacking sequences relating to the structure of NiCl(OH) were trialled, with each run taking days of computing time. The present work addresses the time-consuming computational aspects of the supercell approach and is an extension of the work by Ainsworth *et al.* (2016). Bottlenecks associated with unit cells comprising thousands of atoms resulting in hundreds of thousands of reflections are tackled. In particular the 3 h 1000 repeat Rietveld refinements performed by Ainsworth *et al.* (2016) for averaging of supercells can now be performed in under 1 min.

Rietveld refinement (Rietveld, 1969; Young, 1993) can be broken down into a number of steps: (i) calculation of structure factors, (ii) calculating peaks with intensities obtained from the structure factors, (iii) forming a diffraction pattern using the calculated peaks and (iv) calculating derivatives for



© 2016 International Union of Crystallography

parameters that are refined. We address the challenges associated with each of these steps and then exemplify the computational speed gains possible.

## 2. Calculating structure factors

The structure factor for a particular  $hkl$  of a structure that can be described in terms of stacked layers is the complex quantity

$$F_{\text{str},hkl} = \sum_L \sum_v \sum_a O_{L,a} T_{L,a} (f_{o,L,a} + f'_{L,a} + if''_{L,a}) \times \exp\{2\pi i[\mathbf{h} \cdot (\mathbf{r}_{L,a} + \mathbf{v}_{L,v})]\}, \quad (1)$$

where the subscript  $L$  corresponds to the different layer types,  $v$  to stacking vectors of layer  $L$  and  $a$  to the atoms in layer  $L$ .  $\mathbf{r}_{L,a}$  corresponds to the atom vector position in fractional coordinates,  $T_{L,a}$  the temperature factor,  $O_{L,a}$  the site occupancy,  $f_{o,L,a}$  the atomic scattering factor,  $f'_{L,a}$  and  $f''_{L,a}$  the anomalous dispersion coefficients,  $\mathbf{h}$  the  $hkl$  vector  $\{h, k, l\}$ , and  $\mathbf{v}_{L,v}$  the stacking vector  $\mathbf{v}$  of each layer in fractional coordinates. The stacking vector part of equation (1) can be taken out of the innermost summation, as shown in equation (2), allowing the stacking vector summation to be performed independently of the layer summation:

$$F_{\text{str},hkl} = \sum_L \left\{ \sum_v \exp[2\pi i(\mathbf{h} \cdot \mathbf{v}_{L,v})] \right\} \text{Layer}_{L,hkl},$$

where

$$\text{Layer}_{L,hkl} = \sum_a \text{Atom}_{L,a}$$

and

$$\text{Atom}_{L,a} = O_{L,a} T_{L,a} (f_{o,L,a} + f'_{L,a} + if''_{L,a}) \exp[2\pi i(\mathbf{h} \cdot \mathbf{r}_{L,a})]. \quad (2)$$

In many cases the number of unique  $x$  and  $y$  coordinates  $N_{uxy}$  amongst the stacking vectors  $\{\mathbf{v}_{L,v,x}, \mathbf{v}_{L,v,y}\}$  is small, and equation (2) can be rearranged to reflect this as shown in equation (3) where the summation over  $vxy$  corresponds to stacking vectors with unique  $\{\mathbf{v}_{L,v,x}, \mathbf{v}_{L,v,y}\}$  and the summation over  $u$  corresponds to  $\mathbf{v}_{L,v,z}$  values that all have the same  $\{\mathbf{v}_{L,v,x}, \mathbf{v}_{L,v,y}\}$ . The resulting  $V_{L,hkl}$  is a complex quantity derived from all the stacking vectors as applied to layer  $L$ . Performing the summation of equation (2) using equation (3) can speed up the calculation of  $F_{\text{str},hkl}$  by a factor of 15–20:

$$F_{\text{str},hkl} = \sum_L V_{L,hkl} \text{Layer}_{L,hkl}$$

where

$$V_{L,hkl} = \sum_{vxy} \exp[2\pi i(hv_{x,vxy} + kv_{y,vxy})] \sum_u \exp(2\pi ilv_{z,vxy,u}). \quad (3)$$

For analyses where  $\{\mathbf{v}_{L,v,x}, \mathbf{v}_{L,v,y}\}$  vectors are randomly offset, as in the work of Bette *et al.* (2015), then the speed gain using equation (3) is not possible.

## 3. Obtaining an average intensity from many similarly faulted crystals

To more accurately represent the probabilistic nature of stacking faults using supercells of finite size, an average intensity from many crystals (called structures from here on) can be used. One could perform this averaging from  $N_{\text{str}}$  separate pattern calculations, where  $N_{\text{str}}$  corresponds to the number of structures used, which would require an  $N_{\text{str}}$ -fold increase in computational time. The process can, however, be performed by averaging the intensities as described in equation (4) and then calculating one pattern instead of  $N_{\text{str}}$  patterns:

$$I_{\text{avg},hkl} = (1/N_{\text{str}}) \sum_{\text{str}} |F_{\text{str},hkl}|^2. \quad (4)$$

For structures comprising layer types of various thicknesses, the thickness of each structure will vary because of faulting. A finite and small  $N_v$  would then give  $N_{\text{str}}$  slightly different lattice parameters. Efficient use of equation (4), however, requires the use of a single set of lattice parameters for all structures; for stacking along the  $c$  axis this means using an average  $c$  lattice parameter  $c_{\text{avg}}$ . This allows the use of the same set of  $hkl$  reflections and the same calculated peak shapes in the Rietveld calculations, and means that summing the calculated peaks onto the calculated pattern is performed once and not  $N_{\text{str}}$  times. The neglected smoothing due to a differing lattice parameter can be approximated in a smoothing function described below.

The speed at which  $I_{\text{avg},hkl}$  can be calculated for 100 structures in the generation of a typical powder pattern is only two to three times slower than  $I_{hkl}$  for a single structure; this is demonstrated below. In the theoretical recursive method of Treacy *et al.* (1991) the intensity for a particular faulting probability is treated statistically. The present work achieves a similar effect numerically using  $I_{\text{avg},hkl}$ .

From equations (3) and (4) the computational effort,  $O(I_{\text{avg},hkl})$ , required to calculate  $I_{\text{avg},hkl}$  scales as equation (5):

$$O(I_{\text{avg},hkl}) = N_{\text{str}}(N_v I_{\text{max}} + N_{uxy} N_{hkl}). \quad (5)$$

$I_{\text{max}}$  corresponds to the maximum  $l$  value encountered in the calculation of  $V_{L,hkl}$  in equation (3).

## 4. Generating stacking sequences

In the generation of the stacking sequences from a particular stacking probability matrix, it is advantageous to have  $I_{\text{avg},hkl}$  changing as little as possible. This allows the goodness of fit of multiple Rietveld refinements to be compared as a function of the parameters of the stacking probability matrix. Indeed, the change in the goodness of fit can be determined as a function of the probability parameters and optimization performed in order to determine best-fit values.

Stacking sequences are generated from a stacking probability matrix of the type used in the *DIFFaX* package [Treacy *et al.* (1991); see for example Fig. 9 of Ainsworth *et al.* (2016)]. In an initial step the probability matrix is used to generate  $N_{\text{avg}} N_{\text{str}} N_v$  layers, and from this prediction run the number of

- 1) For each structure generate  $N_v$  layers based on the probability matrix and form a single summation over all structures to produce the summation matrix  $\mathbf{S}_{gen}$  of layer  $i$  to  $j$  transitions.
- 2) Terminate the generation of  $\mathbf{S}_{gen}$  when the following is obeyed for each of its elements:

$$|\mathbf{S}_{pred,i,j} - \mathbf{S}_{gen,i,j}| < q \mathbf{S}_{pred,i,j}^{1/2}$$

where the subscripts  $i$  and  $j$  are over the elements of  $\mathbf{S}$  and  $q = 0.5$ .

- 3) Chose one of the generated structures at random.
- 4) Add a layer to the randomly chosen structure and keep the last  $N_v$  layers.
- 5) Go to step (2).

### Figure 1

Steps used in the generation of stacking sequences for all structures.

each layer  $i$  to  $j$  transition is determined and placed in a summation matrix  $\mathbf{S}$ , which is then divided by  $N_{avg}$  to give  $\mathbf{S}_{pred}$ .  $N_{avg}$  is typically set to 100. Stacking sequences for each structure are then generated according to the steps shown in Fig. 1. This procedure ensures that the generated summation matrix  $\mathbf{S}_{gen}$  closely matches  $\mathbf{S}_{pred}$ , which in turn matches the overall faulting expressed in the transition matrix. The overall time for generating sequences is small compared to the Rietveld calculations. On termination of the generation process an average  $c$  lattice parameter  $c_{avg}$  from the  $N_{str}$  structures is determined and subsequently used in the calculation of peak positions.

## 5. Smoothing ripples and correcting for differing layer thicknesses

For layer types with differing thicknesses the generation scheme in Fig. 1 will produce supercells of slightly varying thicknesses (varying  $c$  lattice parameters), resulting in smearing of the peaks. This smearing is not described by  $I_{avg,hkl}$  (§3) owing to the use of a finite and single  $c_{avg}$  lattice parameter in the calculation of peak position. In addition, stacking-faulted diffraction patterns calculated from small- $N_v$  supercells will contain ripples and oscillations from individual  $hkl$  reflections when the instrument, emission profile and sample aberrations are small. Using  $I_{avg,hkl}$  reduces ripples caused by poor faulting statistics, but does not eliminate the ripples caused by small  $N_v$ . Ainsworth *et al.* (2016) therefore used a large supercell,  $N_v = 5000$ , to minimize both effects and generate a smooth pattern. Being able to reduce  $N_v$  whilst (i) reducing ripples and (ii) describing smearing due to the use of a single  $c$  lattice parameter without degrading the faulted pattern would be hugely beneficial; the number of reflections would be greatly reduced, resulting in much less computer memory allocation and far greater computational speed.

As  $N_v$  increases the number of peaks increase; in particular, stacking along the crystallographic  $c$  axis sees peaks inserted between the  $(h_1, k_1, l_1)$  and  $(h_1, k_1, l_1 + 1)$  peaks where  $(h_1, k_1,$

$l_1)$  are the Miller indices when  $N_v = 1$ . When the distance in  $2\theta$  from  $(h, k, l)$  to  $(h, k, l + 1)$  is less than the step size of the data for all peaks, then the resulting diffraction pattern is smooth. For small  $N_v$  and sharp intrinsic peaks it is possible to produce a smooth pattern comparable to one created with a large  $N_v$  by inserting peaks, irrespective of  $N_v$ , from  $2\theta_{h,k,l}$  to  $2\theta_{h,k,l+1}$  with intensities ranging from  $F_{h,k,l}^2$  to  $F_{h,k,l+1}^2$ . This introduction of peaks can be approximated by convoluting a right trapezoid of size  $d2\theta/dl = (2\theta_{h,k,l} - 2\theta_{h,k,l+1})$  into each  $hkl$  reflection with intensities at its ends corresponding to  $F_{h,k,l}^2$  and  $F_{h,k,l+1}^2$ . Similarly, a right trapezoid of size  $(2\theta_{h,k,l-1} - 2\theta_{h,k,l})$  can be convoluted to insert peaks from  $2\theta_{h,k,l-1}$  to  $2\theta_{h,k,l}$ . This

twin right trapezoidal function can be approximated by a Gaussian centred at  $2\theta_{h,k,l}$  and then shifted by the centroid shift of the twin trapezoid as shown in equation (6a).

Not all peaks should be broadened by  $d2\theta/dl$ . For example, if all layers have the same height, peaks with indices  $(0, 0, nN_v)$  where  $n$  is an integer would not be broadened; nor would other categories of  $(h, k, nN_v)$  peaks depending on the faulting mechanism. When going from a no-faulting case to a faulting case, lattice points with unchanging perpendicular distances to a particular plane will have their corresponding peak remain sharp. One way of testing whether  $(h, k, l)$  should be broadened is by looking at the structure factors. If  $F_{h,k,l-1}^2$  and  $F_{h,k,l+1}^2$  are near zero and  $F_{h,k,l}^2$  is large, then little to no broadening is expected. On the other hand if  $F_{h,k,l-1}^2$ ,  $F_{h,k,l}^2$  and  $F_{h,k,l+1}^2$  are all of a similar intensity then  $d\theta/dl$  broadening is expected. If we assume the broadening is dependent on  $1 - F_{h,k,l}^2 / (F_{h,k,l-1}^2 + F_{h,k,l}^2 + F_{h,k,l+1}^2)$  we arrive at the broadening term  $\Delta_{h,k,l}$  shown in equation (6b):

$$\text{Shift}_{h,k,l} = \left[ \frac{(2\theta_{h,k,l-1} - 2\theta_{h,k,l})F_{h,k,l-1}^2 + (2\theta_{h,k,l+1} - 2\theta_{h,k,l})F_{h,k,l+1}^2}{F_{h,k,l-1}^2 + F_{h,k,l}^2 + F_{h,k,l+1}^2} \right], \quad (6a)$$

$$\Delta_{h,k,l} = \tau d2\theta/dl \left( \frac{F_{h,k,l-1}^2 + F_{h,k,l+1}^2}{F_{h,k,l-1}^2 + F_{h,k,l}^2 + F_{h,k,l+1}^2} \right). \quad (6b)$$

$\tau$  is a parameter that is varied in order to obtain the best fit during refinement.  $\Delta_{h,k,l}$  is small when  $F_{h,k,l-1}^2$  and  $F_{h,k,l+1}^2$  are small and  $F_{h,k,l}^2$  is large; it is large when  $F_{h,k,l-1}^2$ ,  $F_{h,k,l}^2$  and  $F_{h,k,l+1}^2$  are of similar intensity.  $\Delta_{h,k,l}$  corresponds to the FWHM in  $2\theta$  of a Gaussian function convoluted into each peak and  $\text{Shift}_{h,k,l}$  is the shift applied to each convolution. Equations (6a) and (6b) represent a smoothing function that allows small supercells to approximate much larger supercells. In addition to reducing ripples due to a small  $N_v$ , it also approximates the smearing not seen when there are layer types of varying thicknesses and a single set of lattice parameters used.

This approach produces calculated patterns comparable to supercells ten to 20 times larger. Specifically for two cases  $a$  and  $b$  with  $N_{v,a}$  and  $N_{v,b}$  layers, the speed gain in terms of calculating  $I_{\text{avg},hkl}$  using equation (5) is shown in equation (7):

$$\begin{aligned} \text{Gain} &= O_a(I_{\text{avg},hkl})/O_b(I_{\text{avg},hkl}) \\ &= N_{\text{str},a}(N_{v,a}I_{\text{max},a} + N_{\text{uxy},a}N_{hkl,a}) \\ &\quad / [N_{\text{str},b}(N_{v,b}I_{\text{max},b} + N_{\text{uxy},b}N_{hkl,b})], \end{aligned} \quad (7)$$

where  $O(I_{\text{avg},hkl})$  is the computational effort to calculate  $I_{\text{avg},hkl}$ . For cases  $a$  and  $b$  to have similar faulting statistics then  $N_{\text{str},a}N_{v,a} = N_{\text{str},b}N_{v,b}$ . Noting also that  $l_{\text{max},a}/l_{\text{max},b} = N_{v,a}/N_{v,b}$  and  $N_{hkl,a}/N_{hkl,b} = N_{v,a}/N_{v,b}$ , after substitution into equation (7) we get the speed gain shown in equation (8):

$$\text{Gain} = (N_{v,a}I_{\text{max},b} + N_{\text{uxy},a}N_{hkl,a}) / (N_{v,b}I_{\text{max},b} + N_{\text{uxy},b}N_{hkl,b}). \quad (8)$$

For structures with small  $N_{\text{uxy}}$  equation (8) reduces to  $\sim N_{v,a}/N_{v,b}$ . If  $\mathbf{v}_{L,v,x}$  and  $\mathbf{v}_{L,v,y}$  were random values, then  $N_{\text{uxy},a}$  and  $N_{\text{uxy},b}$  would become  $N_{v,a}$  and  $N_{v,b}$  for systems  $a$  and  $b$ , respectively. The speed gain would then be exactly  $N_{v,a}/N_{v,b}$ .

## 6. Calculating derivatives of structural parameters

Derivatives of  $I_{\text{avg},hkl}$  with respect to stacking vector coordinates, atomic coordinates, occupancies, atomic scattering factors, anomalous dispersion coefficients or temperature factors are all necessary in order to refine on the corresponding parameters in a nonlinear least-squares sense. Excluding the stacking vector coordinates, these derivatives can all be calculated using a layer-dependent  $N_{\text{str}} \times N_{hkl}$  matrix calculated for each nonlinear least-squares iteration. Consider the case of calculating the derivative with respect to the fractional atomic coordinate  $r_{L,a,x}$  for atom  $a$  of layer  $L$ . From equation (3) we have

$$\partial I_{\text{avg},hkl} / \partial r_{L,a,x} = 2F_{\text{str},hkl} V_{L,hkl} \text{Atom}_{L,a} 2\pi i h. \quad (9)$$

In each derivative the quantity  $2F_{\text{str},hkl} V_{L,hkl}$  is used. Both  $F_{\text{str},hkl}$  and  $V_{L,hkl}$  are used during the calculation of  $I_{\text{avg},hkl}$  and hence do not need recalculating for the derivatives. Thus, once  $I_{\text{avg},hkl}$  is calculated, determining the derivatives for a structural parameter for a multi-structure refinement takes the same computational effort as for a single-structure refinement. For the stacking vector coordinates, the derivative from equation (3) for the  $x$  coordinate of stacking vector  $v$  becomes

$$\partial I_{\text{avg},hkl} / \partial v_{L,x} = 2F_{\text{str},hkl} \text{Layer}_{L,hkl} \exp[2\pi i(\mathbf{h} \cdot \mathbf{v}_L)] 2\pi i h. \quad (10)$$

Again, both  $F_{\text{str},hkl}$  and  $\text{Layer}_{L,hkl}$  are calculated during the calculation of  $I_{\text{avg},hkl}$  and hence do not need recalculation for stacking vector coordinate derivatives. Even though these derivatives can be calculated in a fast manner, coordinates of the stacking vectors are typically not refined independently as the quality of the data does not support using thousands of such parameters. Instead, thicknesses of layer types might be refined, resulting in fewer than a dozen or so independent parameters.

## 7. Computational effort as compared to traditional Rietveld refinement

Rietveld refinement without the use of stacking vectors requires the explicit definition of atoms in each stacked layer. We can consider the computational effort using a traditional approach [e.g. *TOPAS* Version 4 (Bruker, 2009)] for averaging  $N_{\text{str}} = 100$  structures each with  $N_v = 960$  layers using the  $\text{La}_2\text{O}_2\text{Cu}_{0.667}\text{Cd}_{0.667}\text{Se}_2$  example investigated by Ainsworth *et al.* (2016). Each structure has  $N_{hkl} = 54\,881$   $hkl$  reflections and six layer types  $N_L = 6$ , with four layers having seven atoms per layer and two layers having eight atoms per layer. Each peak shape generated requires  $N_{\text{ops\_per\_pk}} \simeq 2000$  operations and each summation of the peak shape to the calculated pattern requires  $N_{\text{pk\_shape\_sum}} \simeq 150$  operations. The value of  $N_{\text{ops\_per\_pk}} \simeq 2000$  corresponds to a pseudo-Voigt peak shape convoluted with one emission profile line with the instrument aberrations of axial divergence and a receiving slit width (Cheary & Coelho, 1992). The computational effort required to calculate  $I_{\text{avg},hkl}$ ,  $O(I_{\text{avg},hkl})$ , and to calculate the peaks,  $O(\text{Peaks})$ , approximately scales according to equation (11) with all numbers originating from the program itself:

$$\begin{aligned} O(I_{\text{avg},hkl}) &= N_{\text{str}} N_{hkl} \left( \sum_L N_{L,\text{atoms}} \right) N_v / N_L \\ &= 100 \times 54881 \times 44 \times 960 / 6 = 3.86 \times 10^{10}, \\ O(\text{Peaks}) &= N_{hkl} (N_{\text{ops\_per\_pk}} + N_{\text{pk\_shape\_sum}}) \\ &= 54481 \times (2000 + 150) = 1.17 \times 10^8. \end{aligned} \quad (11)$$

The same calculation in *TOPAS* Version 6 with the stacking implementations discussed above reduces to the scaling shown in equation (12):

$$\begin{aligned} O(I_{\text{avg},hkl}) &= N_{hkl} \left( \sum_L N_{L,\text{atoms}} \right) + 2N_{hkl} \left( \sum_L N_{L,\text{atoms}} \right) + N_L (l_{\text{max}} + N_{hkl}) \\ &= 54881 \times 44 + 2 \times 44 \times 54881 + 6 \times (4915 + 54881) \\ &= 7.60 \times 10^6 \\ O(\text{Peaks}) &= N_{\text{pks\_buf}} N_{\text{ops\_per\_pk}} + N_{\text{pks\_summed}} N_{\text{pk\_shape\_sum}} \\ &= 1348 \times 2000 + 11000 \times 150 = 4.34 \times 10^6. \end{aligned} \quad (12)$$

$N_{hkl}(\sum_L N_{L,\text{atoms}})$  corresponds to  $\sum_L \text{Layer}_{L,hkl}$  in equation (2), which relates to the calculation of the structure factors for the six different layers.  $l_{\text{max}}$  corresponds to the maximum  $l$  value encountered in the calculation of  $V_{L,hkl}$  in equation (3).

For  $hkl$ -dependent peak broadening traditional Rietveld programs, for example *TOPAS* Version 5 (Coelho, 2015) and earlier, would require the calculation of  $N_{\text{str}} N_{hkl} = 2.5 \times 10^8$  peaks. *TOPAS* Version 6 uses a peaks buffer that is  $hkl$  dependent (Ainsworth *et al.*, 2016) to greatly reduce the number of peaks calculated. In this example it generates  $N_{\text{pks\_buf}} = 3474$  peaks which is used by the  $N_{\text{str}}$  structures. Summing the peaks from the peaks buffer to form the calculated pattern is also a process that can be streamlined such that peaks of a similar shape that lie between adjacent data points have their intensities appropriated to the adjacent data points. In this manner the number of peaks summed onto the calculated pattern is typically less than the number of data points in the pattern; in the present example  $N_{\text{pks\_summed}} \simeq 11\,000$  as opposed to the number of reflections which is 54 881.



**Table 1**

Average and standard deviation of  $R_{wp}$  over 30 refinements each on *DIFFaX*-simulated diamond data for  $pa = 0.7$  for various  $N_{str}$  and  $N_v$  values.

Refinement range 10–150°  $2\theta$ . The smoothing function was applied to all refinements except for the cases with  $N_v = 5000$ .

$N_{str}$	1	1	200	1000	500	200	10000	5000	200
$N_v$	200	5000	200	100	200	500	100	200	5000
$N_{str} \times N_v$	200	5000	40000	100000			1000000		
$N_{hkl}$	9474	236902	9474	2361	9474	23611	4724	9474	236902
$N_{pks\_buf}$	2532	2760	2532	1122	2532	5305	1122	2532	2760
Average $R_{wp}$ (%)	2.90	1.28	0.509	0.498	0.489	0.483	0.471	0.458	0.465
Standard deviation $R_{wp}$ (%)	0.53	0.17	0.040	0.020	0.025	0.027	0.007	0.006	0.006

Both equations (11) and (12) are approximate in regards to computing time as each operation can amount to four to ten floating-point operations with the actual time taken being hardware dependent; they do, however, give an idea of the magnitude of the computation, especially when comparing the values between equations (11) and (12). For derivatives the computational effort is dependent on which parameters are refined. The number of operations for calculating a peak shape derivative scales by  $O(\text{Peaks})$ ; for structural parameters it scales by  $N_{hkl}$  [see equation (9)] and  $O(N_{pks\_summed} N_{pk\_shape\_sum})$ . Thus even though  $O(N_{pks\_summed} N_{pk\_shape\_sum})$  is relatively small compared to  $I_{avg,hkl}$  of equation (12), it can become significant when many structural parameters are refined.

The resulting computational speed-up of equation (12) compared to traditional Rietveld refinement [equation (11)] is of the order of  $10^4$ ; this would further increase for structures with more atoms in each layer, or for cases where more complex peak shapes are used.

### 8. Test data

Fig. 2 shows the current implementation fitting data generated with the test input file *dia.dat* for stacking-faulted diamond distributed with the *DIFFaX* suite (Treacy *et al.*, 1991) with a 0.7 probability ( $pa$ ) for  $N_v = 200$  and for the cases of  $N_{str} = 1$  and  $N_{str} = 200$ . The much improved fit for  $N_{str} = 200$  (Fig. 2b),  $R_{wp} = 0.51\%$  as opposed to  $R_{wp} = 3.74\%$ , is due to the averaging procedure of equation (4) and the smoothing function of equations (6a) and (6b). No weighting was given to the data during refinement and the formula used to calculate  $R_{wp}$  is shown in equation (13), where  $Y_o$  and  $Y_c$  correspond to observed (here *DIFFaX*-simulated) and calculated intensities:

$$R_{wp} = 100 \left[ \frac{\sum_{m=1}^{N_{data}} (Y_{o,m} - Y_{c,m})^2}{\sum_{m=1}^{N_{data}} (Y_{o,m})^2} \right]^{1/2}. \quad (13)$$

The time taken to perform the first eight iterations for  $N_{str} = 1$  is 1.92 s; for  $N_{str} = 200$  it is 1.99 s. Refinement times, however, depend on what is being refined as various calculated data are saved during refinement and calculated only once. It is therefore more relevant to consider the time taken to calculate the pattern itself; for ten pattern calculations the time for  $N_{str} = 1$  is 0.67 s; for  $N_{str} = 200$  it is 1.26 s; or it is around twice as slow for 200 times more structure-factor calculations. Working with the same *DIFFaX* data of Fig. 2, Ainsworth *et al.*

(2016) used  $N_v = 5000$  stacking vectors but with  $N_{str} = 1$ . Using the input file of Fig. 3 but with these parameters ( $N_{hkl} = 236\,902$ ,  $N_{pks\_buf} = 2760$ ) results in an  $R_{wp}$  of 1.28% and a time to calculate the pattern ten times of 6.8 s. This demonstrates the great benefit of averaging in both computing time and accuracy.

To explore the influence of  $N_{str}$  and  $N_v$  the simulated data were initially fitted with  $N_{str} = 200$  and  $N_v = 5000$  and without the use of the smoothing function; five peak shape parameters, a zero error and one Rietveld scale parameter were initially refined. These large  $N_{str}$  and  $N_v$  values result in a low  $R_{wp}$  of 0.465% as shown in Table 1. The peak shape parameters and zero error were then fixed and the smoothing function of equations (6a) and (6b) included in refinements using

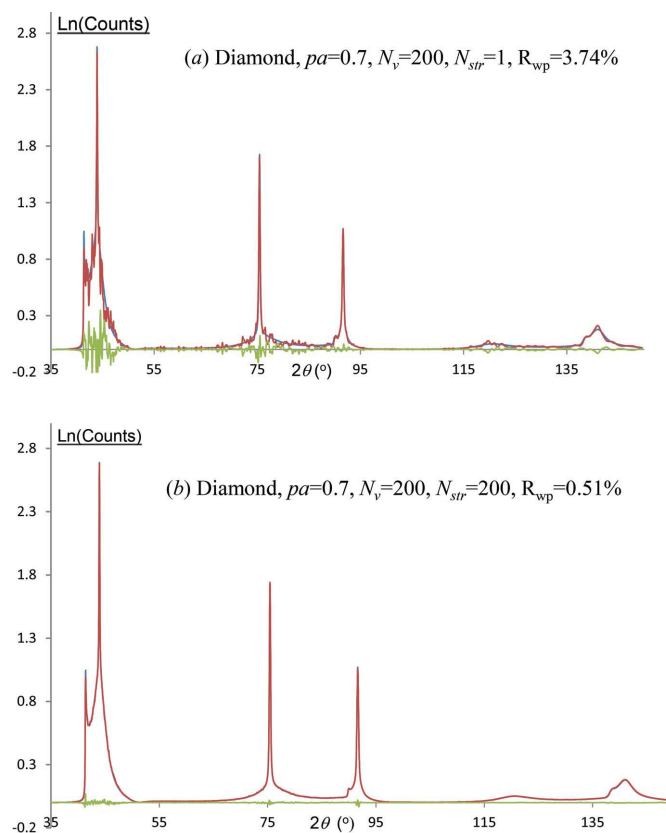


**Figure 2**  
Fit to simulated diamond data from *DIFFaX* for the cases of (a)  $N_{str} = 1$  and (b)  $N_{str} = 200$ . In both cases  $N_{hkl} = 9474$  and  $N_{pks\_buf} = 2532$  peaks. Red, blue and grey lines correspond to calculated, *DIFFaX* simulation and difference plots, respectively.

**Table 2**  
Fractional atomic coordinates used to generate test patterns.

All sites occupied with carbon atoms with an occupancy of 1.

Layer	Atom	<i>x</i>	<i>y</i>	<i>z</i>	<i>B</i> <sub>eq</sub> (Å <sup>2</sup> )
1	C	-1/3	-1/6	-0.125	1
1	C	1/3	1/6	0.125	1
2	C	1/3	1/6	-0.125	1
2	C	-1/3	-1/6	0.125	1

different  $N_{\text{str}}$  and  $N_v$  values; Table 1 shows the results. For equivalent faulting statistics ( $N_{\text{str}} \times N_v$  equal) the  $R_{\text{wp}}$  values are very similar. A reduction in  $R_{\text{wp}}$  is seen as  $N_{\text{str}} \times N_v$  increases. For  $N_v \geq 100$  and for  $N_{\text{str}} \times N_v \geq 100\,000$   $R_{\text{wp}}$  values are similar. The case of  $N_{\text{str}} = 200$ ,  $N_v = 200$  has a marginally

higher  $R_{\text{wp}} = 0.509\%$ , but still with the excellent fit seen in Fig. 2(b). These data demonstrate that small supercells (low  $N_v$ ) can approximate much larger supercells when averaging and the smoothing function of equations (6a) and (6b) are used.

To further test the  $I_{\text{avg}}$  procedure, the test structure described in Table 2 and Fig. 4 was used to generate a complex test pattern with  $pa = 0.7$  and with two different layer heights of 5 and 6 Å ( $\varepsilon = 1$  in Fig. 4), with the other five lattice parameters being  $a = 3$ ,  $b = 4$  Å,  $\alpha = 90$ ,  $\beta = 90$  and  $\gamma = 95^\circ$ . For accuracy, a small step size of  $0.01^\circ 2\theta$  was used and the peak shape comprised a Gaussian instrument function with an FWHM of twice the step size; this results in a pattern that is essentially the aberration function produced from stacking faults. The pattern was generated using a normal Rietveld

calculation averaging 200 individual structures, each with a large supercell comprising  $N_v = 2000$  layers and each with separate  $c$  lattice parameters corresponding to the overall heights of the stacked layers. Each unit cell therefore comprised  $2000 \times 4 = 8000$  atoms for a total of 1 600 000 atomic sites in the calculation. The calculation was performed out to  $40^\circ 2\theta$  which encompassed 28 325 reflections. This translates to an innermost loop for the calculation of structure factors that is executed  $1\,600\,000 \times 28\,325 = 45\,176\,000\,000$  times; the pattern calculation time was long at 1828 s. Fitting to this test pattern using  $I_{\text{avg}}$  with  $N_{\text{str}} = 200$  and  $N_v = 2000$  (identical faulting statistics to the generation procedure) produces the good fit shown in Fig. 5 where  $R_{\text{wp}} = 3.27$  (20)%; the calculation time for the first iteration was only 1.2 s. The nonzero  $R_{\text{wp}}$  is due to the faulting statistics represented by the transition probability matrix and remaining minor ripples in the (instrument/sample unbroadened) test pattern. Setting  $N_v = 400$  and using the smoothing function of equations (6a) and (6b) results in  $R_{\text{wp}} = 4.08$  (25)% and a tenfold faster calculation of 0.12 s. Thus  $I_{\text{avg}}$  correctly describes the Rietveld-generated pattern with two layer heights in an extremely fast manner when a relatively small  $N_v$  is used together with the smoothing function.

To further show the benefits of the smoothing function of equations (6a) and (6b) the same structure but with  $\alpha = 75$ ,  $\beta = 85$  and  $\gamma = 95^\circ$  was used to generate a test pattern out to  $150^\circ 2\theta$ ; no smoothing function was used and the

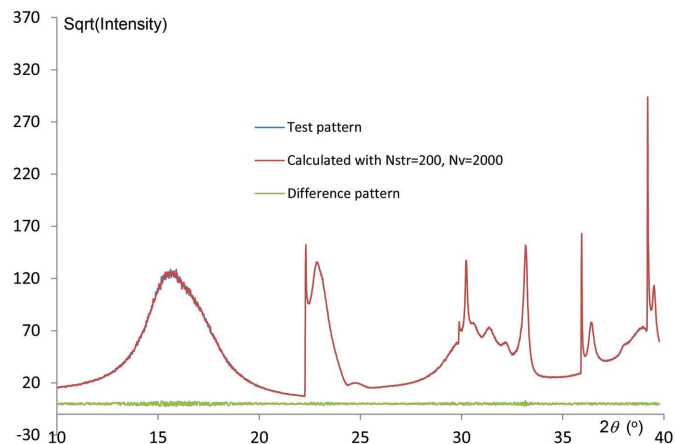
```
xdd diffax_dia.xy
LP_Factor(0) bkg 1
start_X 10 finish_X 149.6
rebin_with_dx_of 0.01
lam ymin_on_ymax 0.0001 la 1 lo 1.5405754 lh 1e-5
Zero_Error(@, 0.0025)
weighting 1
str
  space_group P1
  a 2.518156 b 2.518156 c = Get(generated_c); ga 120
  prm !pa 0.7 prm !h 2.05870
  prm s 1 min 1e-15 scale = s 1e-6 / (Nv Nstr);
  generate_stack_sequences {
    number_of_sequences Nstr 200
    number_of_stacks_per_sequence Nv 5000
    Transition(A, h)
      to A = pa; a_add = 2/3; b_add = 1/3;
      to B = 1-pa; a_add = 0; b_add = 0;
    Transition(B, h)
      to A = 1-pa; a_add = 0; b_add = 0;
      to B = pa; a_add = -2/3; b_add = -1/3;
  }
  site C1 x = -1/3; y = -1/6; z = -0.125/Nv; occ C 1 beq 1 layer A
  site C2 x = 1/3; y = 1/6; z = 0.125/Nv; occ C 1 beq 1 layer A
  site C3 x = 1/3; y = 1/6; z = -0.125/Nv; occ C 1 beq 1 layer B
  site C4 x = -1/3; y = -1/6; z = 0.125/Nv; occ C 1 beq 1 layer B
  peak_buffer_based_on = Xo; peak_buffer_based_on_tol 0.1
  TCHZ_Peak_Type(@,0.01,@,-0.01,@,0.01,@,0,@,0.1,@,0.01) 'Instrument function
```

**Figure 3**  
Input file used for fitting to *DIFFA*X diamond data for  $N_{\text{str}} = 200$  and  $N_v = 5000$ .

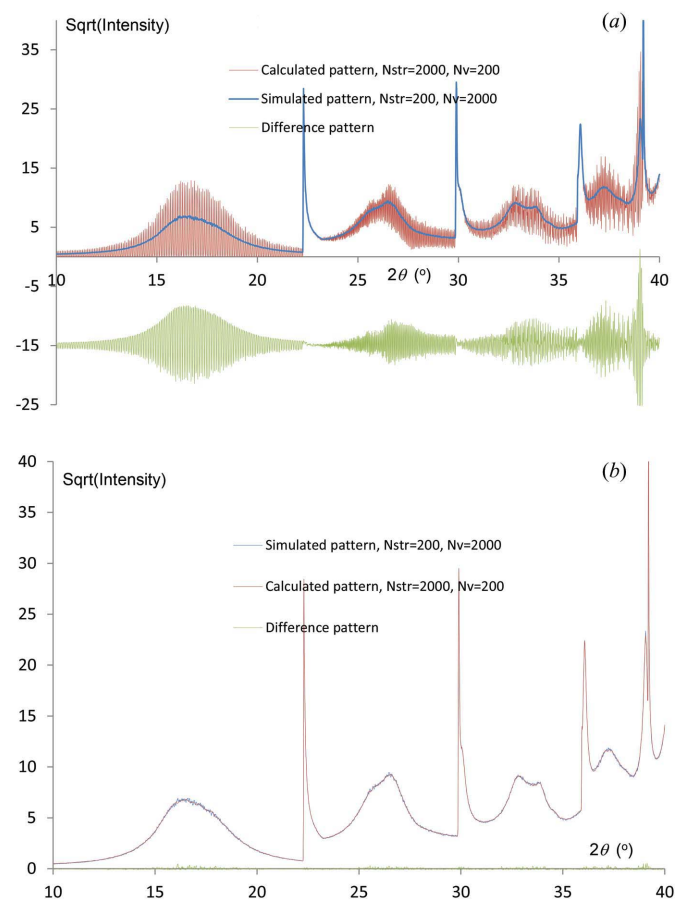
```
From layer 1
  To layer 1 with a probability of pa and shifted by the vector {2/3,1/3,c/Nv}
  To layer 2 with a probability of 1-pa and shifted by the vector {0,0,c/Nv}
From layer 2
  To layer 1 with a probability of 1-pa and shifted by the vector {2/3,0,(c+ε)/Nv}
  To layer 2 with a probability of pa and shifted by the vector {2/3,2/3,(c+ε)/Nv}
```

**Figure 4**  
Transition matrix and stacking vectors used to generate test patterns. Shifts in the  $ab$  plane are expressed in fractional coordinates, those along the stacking direction in Å.

pattern was again generated using  $I_{\text{avg}}$  with  $N_{\text{str}} = 200$  and  $N_v = 2000$ . Fitting to this test pattern with the same faulting statistics (equal  $N_{\text{str}} \times N_v$ ) we put  $N_{\text{str}} = 2000$  and  $N_v = 200$ . Fig. 6(a) shows the poor fit when the smoothing function is not used.



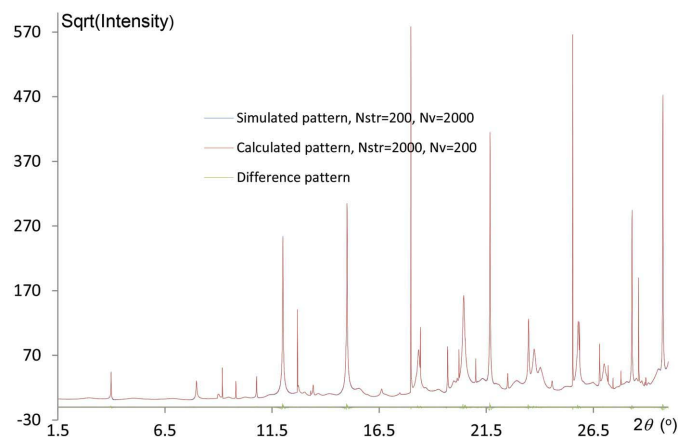
**Figure 5** Fit to Rietveld-generated pattern comprising 200 structures each with 2000 layers and each with its own  $c$  lattice parameter determined from the different layer thicknesses and faulting. The calculated pattern used the  $I_{\text{avg}}$  implementation with a single  $c$  lattice parameter.



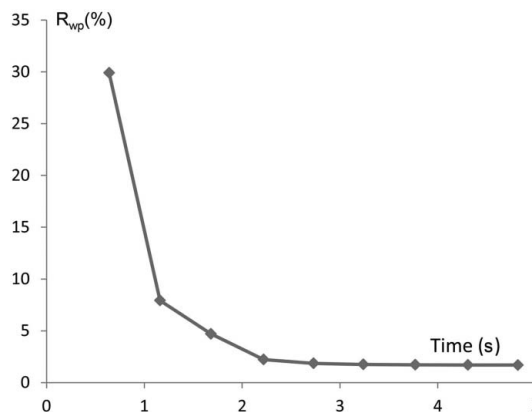
**Figure 6** Fit to a simulated test pattern created with  $N_v = 2000$  and no smoothing function using a calculated pattern created with  $N_v = 200$  for the cases (a) with no smoothing function and (b) with the smoothing function.

Fig. 6(b) shows the fit when the smoothing function is used, resulting in  $R_{\text{wp}} = 1.77$  (13)% out to  $150^\circ 2\theta$ . Setting  $N_{\text{str}} = 200$  gives an  $R_{\text{wp}} = 1.82$  (5)%. Thus, the smoothing function with a small supercell accurately describes much larger supercells for the complex case of varying layer heights.

Fig. 7 shows the fit to a simulated pattern of the  $\text{La}_2\text{O}_2\text{Cu}_{0.667}\text{Cd}_{0.667}\text{Se}_2$  structure reported by Ainsworth *et al.* (2016) which comprised three layer types. The simulated pattern used a step size of  $0.005^\circ 2\theta$ , peak shapes set to a Gaussian with an FWHM of  $0.01^\circ 2\theta$ ,  $N_{\text{str}} = 200$  and  $N_v = 2000$ , and no smoothing function. The calculated pattern for  $N_{\text{str}} = 2000$  and  $N_v = 200$  with the smoothing function resulted in  $R_{\text{wp}} = 1.335$  (39)%; setting  $N_{\text{str}} = 200$  and  $N_v = 200$  gives  $R_{\text{wp}} = 1.63$  (27)%. These  $R_{\text{wp}}$  values can be compared to 1.45% for  $N_{\text{str}} = 200$  and  $N_v = 2000$  (same values as those used for the simulated pattern; nonzero  $R_{\text{wp}}$  due to the faulting statistics). Fig. 8 shows  $R_{\text{wp}}$  as a function of iteration time from Rietveld refinement using  $I_{\text{avg}}$ , the smoothing function,  $N_{\text{str}} = 200$  and  $N_v = 200$  for the  $\text{La}_2\text{O}_2\text{Cu}_{0.667}\text{Cd}_{0.667}\text{Se}_2$  test pattern. The refinement range was set to  $1.5\text{--}30^\circ 2\theta$ , resulting in 41 272 reflections. The refinement comprised 15 site coordinate



**Figure 7** Fit to a simulated  $\text{La}_2\text{O}_2\text{Cu}_{0.667}\text{Cd}_{0.667}\text{Se}_2$  test pattern created with  $pa = 0.3$ ,  $N_v = 2000$  and no smoothing function using a calculated pattern with  $N_v = 200$  and with the smoothing function.



**Figure 8**  $R_{\text{wp}}$  versus time from Rietveld refinement of a test  $\text{La}_2\text{O}_2\text{Cu}_{0.667}\text{Cd}_{0.667}\text{Se}_2$  pattern. The refinement used  $N_{\text{str}} = 200$  and  $N_v = 200$ .



**Table 3**

Average and standard deviation of  $R_{wp}$  and  $pa_{gen}$  over 500 refinements for  $La_2O_2Cu_{0.667}Cd_{0.667}Se_2$  [data from Ainsworth *et al.* (2016)] for various  $N_{str}$  and  $N_v$  values.

Refinement range 1.5–20° 2 $\theta$ . The approximate relative time required for each of the 500 refinements is given.

$N_{str}$	1	100	200	1	25	100	200
$N_v$	960	960	960	192	192	192	192
$N_{hkl}$	54877	54877	54877	10973	10973	10973	10973
$N_{pks\_buf}$	3474	3474	3474	1326	1326	1326	1326
Average $R_{wp}$ (%)	3.014	2.933	2.933	3.591	2.780	2.751	2.748
Standard deviation $R_{wp}$ (%)	0.146	0.010	0.008	0.662	0.044	0.019	0.014
$pa_{gen}$	0.0096	0.01103	0.01101	0.009	0.0109	0.01101	0.01101
Standard deviation $pa_{gen}$	0.0014	0.00012	0.00008	0.006	0.0006	0.00025	0.00022
Time (s)	0.71	1.33	1.96	0.45	0.49	0.56	0.66

parameters, three layer height parameters, one lattice parameter, one Rietveld scale parameter and  $\tau$  from the smoothing function of equation (6b). Layer height parameters were initially set to  $\sim 0.05$  Å from their optimal values. Fig. 8 shows the fast convergence of these stacking vector parameters. The 5 s to refinement convergence is significant as it allows for hands-on real-time analysis of such data sets.

These test data suggest that large  $N_v$  supercells are not necessary to fit complex patterns. In addition, real data have considerable intrinsic broadening due to instrument, emission profile and specimen-type aberrations such as crystallite size and strain broadening. Thus, even though the smoothing function of equations (6a) and (6b) is important in allowing small- $N_v$  fits to simulated test data with narrow intrinsic peaks, the need with real data is lower.

## 9. Real data analysis

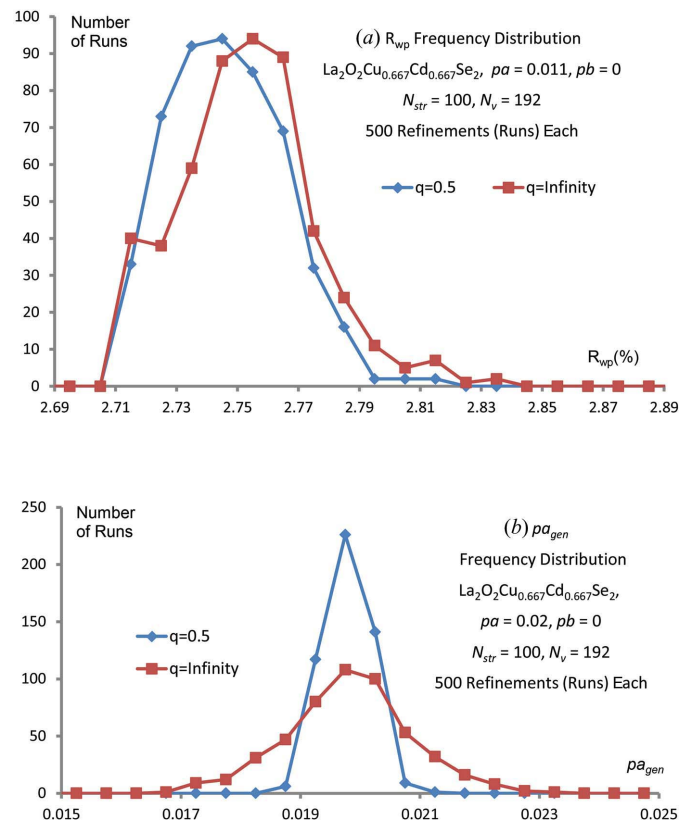
We can further explore the speed and accuracy gains enabled by these developments using one of the data sets described by Ainsworth *et al.* (2016). We choose the  $La_2O_2Cu_{0.667}Cd_{0.667}Se_2$  composition discussed above, which is a layered oxychalcogenide that can be described in terms of alternating fluorite-like  $[La_2O_2]^{2+}$  slabs and either  $[CdSe_2]^{2-}$  or  $[Cu_2Se_2]^{2-}$  anti-fluorite-derived slabs. The ideal structure has a 2:1 ordered sequence of metal chalcogenide layers (Cd1|Cd2|Cu3|Cd4|Cd5|Cu6), where each underlined Cd layer is offset by  $(a/2, b/2)$ . Two types of faults were investigated: a  $pa$ -type fault involving an additional layer of either metal to form local (Cu|Cu|Cd|Cd) or (Cu|Cd|Cd|Cd) sequences; and a  $pb$  fault involving Cd layers being offset by  $(a/2, b/2)$  either side of a Cu layer. In the original paper the dependence of  $R_{wp}$  on fault probabilities  $pa$  and  $pb$  was investigated using a model with six  $[LaOLaSe(Cu_2/Cd)Se]$  layers (three unique) stacked to form a supercell with 960 layers in total ( $N_{str} = 1, N_L = 6, N_v = 960$ ).

Firstly, we investigate the stacking generation method as a function of the constant  $q$  described in step (2) of Fig. 1. Fig. 9(a) shows the frequency distribution of  $R_{wp}$  for 500 Rietveld refinements for the cases of  $q = 0.5$  and  $q = \infty$ ; in the latter case there is no constraint on the number of faults generated in the structures and the average  $R_{wp}$  is slightly larger than the value for  $q = 0.5$ . Fig. 9(b) shows corresponding

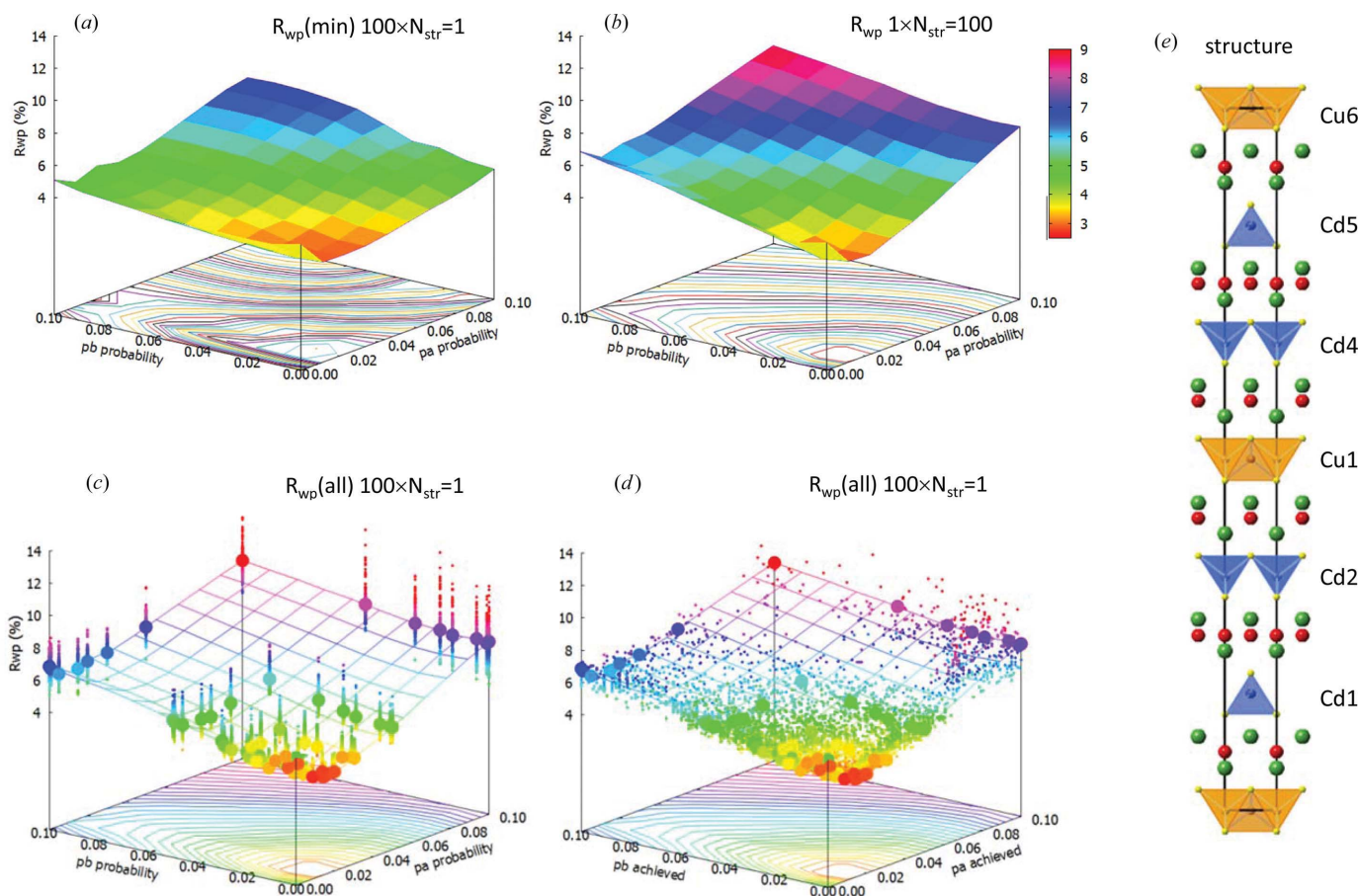
generated  $pa$  values  $pa_{gen}$ ; a much narrower spread in  $pa_{gen}$  is found for  $q = 0.5$  as expected. For this reason  $q = 0.5$  is used in the analysis below.

Table 3 shows the influence of different values for  $N_{str}$  and  $N_v$  on  $R_{wp}$  and  $pa_{gen}$  using our averaging approach. Fig. 10 shows the influence of different  $N_{str}$  values for the  $R_{wp}$  surfaces obtained for  $N_v = 960$  with  $pa$  and  $pb$  values between 0.0 and 0.1 with different procedures. Fig. 10(a) shows the surface of minimum  $R_{wp}$  values obtained from 100  $N_{str} = 1$  trial structures for each of

64  $pa/pb$  combinations as reported in the original paper. The entire surface took around 15 h to calculate on an i7 3.4 GHz single-core desktop computer. Fig. 10(b) shows the equivalent  $R_{wp}$  surface determined using our averaging processes with  $N_{str} = 100$ , which took 160 s on the same computer. The speed gain is a combination of the smaller number of refinements required (64 *versus* 6400), the use of a more efficient algorithm to create constrained stacking sequences and other improvements to *TOPAS*. A more direct comparison of the speed gain from averaging can be obtained by comparing the time to perform  $64 \times 100$  refinements with  $N_{str} = 1$  ( $\sim 8000$  s) with that to carry out 64  $N_{str} = 100$  refinements (160 s). A speed gain of



**Figure 9** Frequency distribution from two sets of refinements,  $q = 0.5$  and  $q = \infty$ , each comprising 500 refinements of  $La_2O_2Cu_{0.667}Cd_{0.667}Se_2$  with  $N_{str} = 100$  and  $N_v = 192$  for (a)  $R_{wp}$  and for (b)  $pa_{gen}$ .

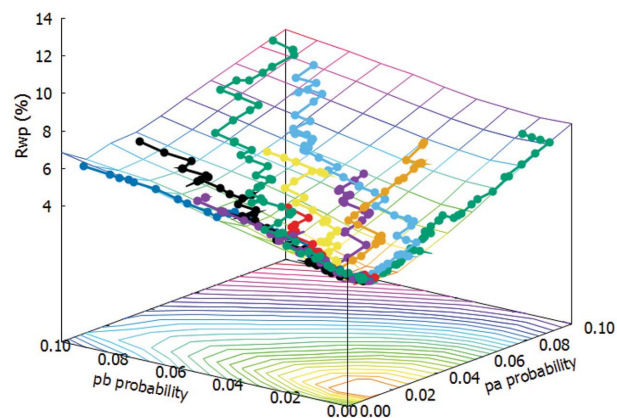

**Figure 10**

Three-dimensional plots showing  $R_{wp}$  values for refinements of different  $\text{La}_2\text{O}_2\text{Cu}_{0.667}\text{Cd}_{0.667}\text{Se}_2$  stacking models. (a) The minimum  $R_{wp}$  value from 100 repeat refinements of models with  $N_v = 960$  and  $N_{str} = 1$  and different  $pa/pb$  values. (b) The  $R_{wp}$  value from single models with  $N_v = 960$  and  $N_{str} = 100$ . (c) A plot of the 100  $R_{wp}$  values for  $N_{str} = 1$  (small points) and the single value for  $N_{str} = 100$  (large points). (d) Same as (c) but with data plotted against the actual number of faults generated in each sequence. The same  $z$  range and colouring are used in each plot. Lines in (c) and (d) are to guide the eye. (e) The structure in terms of  $[\text{La}_2\text{O}_2]^{2+}$  (green/red),  $[\text{CdSe}_2]^{2-}$  (blue/yellow) and  $[\text{Cu}_2\text{Se}_2]^{2-}$  (brown/yellow) slabs.

around 50-fold is observed, as expected from the discussion above. Using the convolution approach of §5 an equivalent surface can be calculated for  $N_v = 96$  in around 20 s.

The averaging process with  $N_{str} = 100$  also leads to a much better defined minimum in the  $R_{wp}$  surface, as shown by the contour levels and minimum–maximum  $R_{wp}$  ranges in Figs. 10(a) and 10(b) (2.80–7.02% and 2.71–8.59%, respectively). The flatter surface in Fig. 10(a) arises from the range of  $R_{wp}$  values encountered for different individual  $N_{str} = 1$  sequences. Fig. 10(c) shows this effect by superimposing the single  $R_{wp}$  value from the  $N_{str} = 100$  refinement (large points and surface mesh) with the 100  $R_{wp}$  values from  $N_{str} = 1$  refinements (small points). For each set  $pa/pb$  combination we see a vertical ‘rod’ of  $R_{wp}$  values reflecting the random nature of the individual stacking sequences generated in each structure. Close to the overall  $R_{wp}$  minimum the  $N_{str} = 100$  refinements lie at the minimum of these rods. For larger  $pa/pb$  values some  $N_{str} = 1$  refinements show a lower  $R_{wp}$ , but this is due to individual structures having fewer faults than the expectation value. Fig. 10(d) shows an equivalent plot to Fig. 10(c), but with  $R_{wp}$  values for the  $N_{str} = 1$  refinements

plotted against the actual number of faults present in each stack. On this plot  $N_{str} = 100$  models lie essentially on the minimum- $R_{wp}$  surface. This plot also shows that  $N_{str} = 1$   $R_{wp}$


**Figure 11**

Minimization pathway using a simple downhill algorithm. Minimization pathways from ten different random starting points shown on an equivalent surface to that of Fig. 10(b).

values have significant scatter; around the  $R_{wp}$  minimum individual  $R_{wp}$  values can be up to 1% higher than the lowest value.

As expected from the smooth  $R_{wp}$  surfaces in Fig. 10, it is relatively straightforward to directly optimize values of  $pa$  and  $pb$ . There are a number of ways of doing this based on Monte Carlo or simulated annealing type approaches (e.g. Bette, 2015). Here a straightforward downhill or greedy algorithm is effective. Fig. 11 shows typical minimization pathways for this problem. Each minimization was complete in a few minutes of computer time.

## 10. Conclusion

In conclusion we show how the use of efficient algorithms for calculating structure factors, efficient pattern averaging, speed-ups in powder pattern calculation using a peaks buffer, a smoothing procedure that allows for the use of much smaller supercells and efficient stacking algorithms lead to massive speed gains in the Rietveld analysis of stacking-faulted structures. Real speed gains of the order of  $10^4$  have been obtained, allowing rapid combined structural and microstructural analysis of complex systems. These processes have been implemented in a general way in the computer program

*TOPAS* Version 6, and we believe they will have wide applicability.

## References

- Ainsworth, C. M., Lewis, J. W., Wang, C., Coelho, A. A., Johnston, H. E., Brand, H. E. A. & Evans, J. S. O. (2016). *Chem. Mater.* **28**, 3184–3195.
- Bette, S., Dinnebier, R. E. & Freyer, D. (2015). *J. Appl. Cryst.* **48**, 1706–1718.
- Bruker (2009). *DIFFRACplus TOPAS4.2*. Technical Reference Manual. Bruker AXS, Karlsruhe, Germany.
- Bruker (2015). *TOPAS*. Version 6.0. Bruker AXS, Karlsruhe, Germany.
- Cheary, R. W. & Coelho, A. (1992). *J. Appl. Cryst.* **25**, 109–121.
- Coelho, A. A. (2015). *TOPAS Academic*. Version 5. <http://www.topas-academic.net>.
- Lutterotti, L., Voltolini, M., Wenk, H. R., Bandyopadhyay, K. & Vanorio, T. (2010). *Am. Mineral.* **95**, 98–103.
- Rietveld, H. M. (1969). *J. Appl. Cryst.* **2**, 65–71.
- Treacy, M. M. J., Newsam, J. M. & Deem, M. W. (1991). *Proc. R. Soc. A Math. Phys. Eng. Sci.* **433**, 499–520.
- Ufer, K., Roth, G., Kleeberg, R., Stanjek, H., Dohrmann, R. & Bergmann, J. (2004). *Z. Kristallogr.* **219**, 519–527.
- Wang, X., Hart, R. D., Li, J., McDonald, R. G. & van Riessen, A. (2012). *J. Appl. Cryst.* **45**, 1295–1302.
- Young, R. A. (1993). Editor. *The Rietveld Method: Introduction to the Rietveld Method*, pp. 1–39, IUCr Monographs on Crystallography. Oxford University Press.